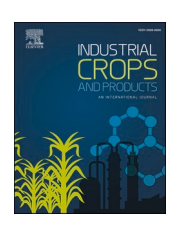
ELSEVIER

Contents lists available at ScienceDirect

Industrial Crops & Products

journal homepage: www.elsevier.com/locate/indcrop





A composition-based model for rapid prediction of pineapple leaf fibers fineness and tensile strength

Shiyu Liao a, Jianming Chen a,b,*, Xungai Wang a,b,*

- a Joint Research Centre for Fiber Innovations and Renewable Materials, School of Fashion and Textiles, The Hong Kong Polytechnic University, Hong Kong, China
- ^b Research Centre of Textiles for Future Fashion, The Hong Kong Polytechnic University, Hong Kong, China

ARTICLE INFO

Keywords:
Pineapple leaf fibers
Degumming
Fiber fineness
Tenacity
Prediction model

ABSTRACT

Pineapple leaf fibers (PALFs) are sustainable resources with exceptional tenacity, yet their component-structure-property relationships remain underexplored, limiting high-value applications. This study establishes quantitative links between chemical composition (cellulose, hemicellulose, lignin) and mechanical properties of single PALFs, aiming to develop a predictive model for rapid fineness and strength assessment. Using stepwise chemical degumming, we generated 11 distinct fiber groups (SSD1–11) from Queen PALF and characterized > 600 fibers via standardized mechanical testing (GB/T5881–2024). Pearson and Mantel correlation analysis revealed a hierarchical component-function framework: cellulose governs PALF stiffness via crystalline microfibrils; hemicellulose modulates fineness and interfacial adhesion as bonding network; lignin enhances stretchability and strength via stress-transfer structure. Critically, we developed a computational model, termed Prediction of Fineness and Strength of Single PALF (PFS-PALF) for rapid assessment, which was experimentally validated to achieve 95 % similarity versus national standard measurements. This approach has potential to replace the conventional labor-intensive and tedious measurements on PALF's mechanical behavior. In addition, PFS-PALF enables reverse regulation of PALFs' composition through optimized degumming parameters and facilitates rapid selection of suitable PALF variety to meet application-specific mechanical requirements.

1. Introduction

Pineapple leaf fibers (PALFs) are increasingly recognized as sustainable alternatives in composites and textiles, owing to their intrinsic antibacterial properties, renewable abundance and reduced environmental footprint. Structurally, PALFs exhibit a hierarchical architecture wherein cellulose microfibrils serve as reinforcing elements embedded within a lignin-hemicellulose matrix (Jose et al., 2016; Mazumder and Zhang, 2023). Conventional studies on PALF mechanical behavior have predominantly focused on fiber bundles, which demonstrate an elastic modulus (37-86 GPa) comparable to E-glass fibers (30-70 GPa) (Manaia et al., 2019; Neto et al., 2015). Despite this competitive stiffness, the industrial utilization of these thick bundles is constricted by inherent limitations, including structural defects, high gum content, and non-uniform cross-sectional geometry (Gaba et al., 2021; Tang et al., 2024; Teles et al., 2015). Although these bundles can be spun into yarns or incorporated into thermoplastic composites (Smitthipong et al., 2015), issues such as inconsistent fineness, surface tension and poor polymer infiltration frequently result in suboptimal mechanical performance (Chollakup et al., 2011; Han et al., 2024). By contrast, single PALFs are of growing interest to composite and textile industries due to their lower linear density and surface free energy, larger contact angle and interfacial binding capabilities (Han et al., 2024). This superiority arises from the homogeneous morphology of single fibers and increased density of surface hydroxyl groups (Shen et al., 2022), which together improve fiber-matrix compatibility. Specifically, degummed finer fibers facilitate uniform distribution within composite matrices, while linear density directly affects yarn quality.

However, achieving rapid and reliable evaluation of single PALF fineness and tensile strength remains a persistent challenge due to labor-intensive conventional protocols. First, PALFs exhibit inherent structural heterogeneity: approximately 56 % of which originates from mesophyll cells with small lumens, whereas the remaining 44 % from vascular tissues characterized by larger, more porous lumens (Surajarusarn et al., 2019). This structural divergence, compounded by variations in chemical composition (e.g., cellulose/lignin ratios)

E-mail addresses: lesley.liao@connect.polyu.hk (S. Liao), jianming.chen@polyu.edu.hk (J. Chen), xungai.wang@polyu.edu.hk (X. Wang).

https://doi.org/10.1016/j.indcrop.2025.121516

Received 4 June 2025; Received in revised form 8 July 2025; Accepted 10 July 2025 Available online 18 July 2025

^{*} Corresponding authors at: Joint Research Centre for Fiber Innovations and Renewable Materials, School of Fashion and Textiles, The Hong Kong Polytechnic University, Hong Kong, China

influenced by plant variety and geographical conditions, results in significant disparities in fiber fineness and mechanical properties (Neto et al., 2013; Radoor et al., 2020). Such variability necessitates repetitive testing (typically >50 replicates per group) to obtain reliable benchmarks, underscoring the critical need for rapid predictive methodologies to streamline single fiber's evaluation. Second, although previous studies have advanced the characterization of individual bast fibers, research specifically addressing single PALF remains scarce. For instance, Sinon et al. conducted systematic measurements of ultimate Abaca fibers, demonstrating that tenacity and fineness are critically dependent on stalk position and variety, emphasizing the importance of source-specific fiber selection (Sinon et al., 2011). Similarly, the measurements on single flax and jute fibers revealed strong correlations between tensile properties, structure and composition (Aldroubi et al., 2023; Wang et al., 2009). Notably, ramie studies developed quadratic regression models to predict breaking strength directly from fiber fineness, showcasing the potential of predictive tools to reduce testing complexity (Leng et al., 2023). So far, models have been rarely established for single PALF to predict its mechanical properties or impact

This study addresses the gap by systematically analyzing the mechanical performance of Queen PALF, one of the most widely cultivated varieties, at various degumming levels. Through controlled stepwise degumming and evaluation of more than 600 samples, we established the relationships among fiber components, crystalline structure parameters, and mechanical properties. Furthermore, robust predictive models (referred to as PFS-PALF) are developed through correlation analysis to rapidly assess single PALF's fineness and mechanical behavior based on its structural composition, providing an efficient alternative to conventional labor-intensive testing. Critically, the model's generalizability was validated across additional three major PALF cultivars (MD-2, Red Spanish and Smooth Cayenne), enabling performance ranking and application-specific selection. For instance, MD-2 for high-strength composites versus Queen for flexible textiles. By linking target mechanical thresholds to chemical composition, this PFS-PALF model enables tailored degumming of PALF, thereby maximizing fiber performance. These advancements deepen the understanding of PALF intrinsic properties and facilitate the development of sustainable high value-added products.

2. Materials and methods

2.1. Materials and sample preparation

The pineapple leaf fibers referred to as Queen and Red Spanish PALF, were obtained from the pineapple planting base of the South Subtropical Crops Research Institute, CATAS, located in Zhanjiang City, Guangdong province, China. MD-2 PALF was provided by University Putra Malaysia, and Smooth Cayenne PALF was sourced from Saeng Charoen Grand Co., Ltd. The chemical reagents used in experiments were acetone (CH₃COCH₃, 99.8 %), ammonium oxalate ((NH₄)₂C₂O₄ 98.0 %), aqueous sulfuric acid (H₂SO₄, 95.0 %), barium chloride (BaCl₂, 99.0 %), sodium chlorite (NaClO₂, 31 % in H₂O), acetic acid (CH₃COOH, 99.0 %), sodium hydroxide (NaOH, 96 %), ammonium hydroxide solution (NH₄OH, 25.0–28.0 %) and absolute ethyl alcohol (C₂H₅OH,99.9 %), purchased from Dieckmann Chemical Industry Co., Ltd., HK; Deionized water (H₂O), deionized by the GenPure Water Purification System, was supplied from the laboratory. All the chemicals were used as received without any further purification.

2.2. Sample preparation

The long PALFs underwent a stepwise chemical degumming process and chemical constituents test, as detailed in our recently published study (Liao et al., 2025), which was developed to selectively remove non-cellulosic constituents. Through systematic parameter

optimization, 11 distinct fiber groups (SSD-1 to SSD-11) were generated, representing incremental degumming intensities. As detailed in Table 1, SSD-2 to SSD-8 were prepared by removing individual gum components relative to the untreated control (SSD-1), enabling isolation of each constituent's effect on mechanical properties. By contrast, SSD-9 to SSD-11 involved sequential multi-component removal, inducing synergistic effects that amplified alterations in fiber fineness and mechanical behavior. This hierarchical design facilitated quantitative identification between primary and secondary compositional influences during correlation analysis.

2.3. Physical properties test of single PALF

Physical characterization of single PALF was conducted after carding in accordance with the standard *GB/T 5881–2024 Test methods for physical and chemical properties of ramie fiber*. The linear density (D) was calculated using Eq. (1).

$$D = \frac{m \times 10^4}{L \times n} \# \tag{1}$$

where: D was the linear density (dtex), m is the mass of the fiber specimen(mg), L is the length of the fiber specimen (mm), and n is the number of individual fibers in the specimen.

Mechanical properties were evaluated using an Instron Universal Testing Machine (Instron 5566) under controlled environmental conditions ($20\pm2^{\circ}$ C, 65 ± 2 % relative humidity). Testing parameters were configured as follows: Strain rate of 10 mm/min, gauge length of 30 mm, and precision load cell with 1020 cN capacity. Key mechanical parameters assessed included specific tenacity, tensile strain, and Young's modulus, providing a comprehensive understanding of PALF's resistance to fracture and elastic deformation. Statistical reliability was ensured by analyzing a minimum of 50 valid individual fibers per sample group after excluding specimens with incomplete separation or non-conforming fracture surfaces. All specimens were preconditioned for 24 h under standard testing conditions to ensure moisture balance prior to measurement.

2.4. Definition of correlation evaluation metric

After obtaining the chemical constituents of PALF, widely used statistical metrics were employed for correlations analysis as follows, which is necessary for developing prediction models.

2.4.1. Pearson correlation analysis

Pearson correlation coefficient is commonly used to reveal the correlations between two variables. Accordingly, the interrelationships between PALF chemical constituents were quantified using Pearson product-moment correlation analysis. This statistical approach calculated the correlation coefficients (r) between five key chemical components: cellulose, hemicellulose, lignin, pectin and others (i.e., fat, wax and water-soluble materials). The results were used to determine the chemical composition dependencies within the PALF.

2.4.2. Mantel test analysis

The Mantel Test was utilized to explore the correlation between the chemical components and the mechanical properties (tenacity, Young's modulus, and tensile strain), as well as the fineness of PALF (linear density). During the test, the statistical significance was determined by permutation testing with distance-based matrices. In this way, the significant predictors can be identified based on the statistical significance, so that the fibers' physical performance can be further refined through targeted adjustments in chemical composition.

2.4.3. Multiple linear regression

To elucidate the linear relationships between the complex chemical

Table 1Chemical compositions of Queen PALF under various degumming conditions.

Sample Group	Description	Cellulose	Hemicellulose	Lignin	Pectin	Others*
SSD-1	Raw Queen PALF	61.9 %	22.1 %	6.6 %	8.0 %	1.5 %
(Control group)						
SSD-2	8 h removal of fat and wax	66.5 %	21.7 %	8.4 %	3.5 %	0.6 %
SSD-3	3 h removal of pectin	67.1 %	23.3 %	8.0 %	0	3.0 %
SSD-4	4 h removal of lignin	66.2 %	22.6 %	2.2 %	2.9 %	8.3 %
SSD-5	8 h removal of lignin	66.0 %	23.0 %	0	3.0 %	8.8 %
SSD-6	4 h removal of hemicellulose	75.1 %	4.1 %	16.3 %	0.7 %	3.8 %
SSD-7	8 h removal of hemicellulose	75.6 %	4.0 %	16.9 %	0.6 %	3.3 %
SSD-8	12 h removal of hemicellulose	81.0 %	0	17.1 %	0.6 %	3.3 %
SSD-9 [#]	8 h removal of lignin	76.8 %	22.5 %	0.3 %	0	0
$SSD-10^{\#}$	2 h removal of hemicellulose	83.1 %	5.0 %	10.0 %	0	0
SSD-11 [#]	8 h removal of lignin, 2 h removal of hemicellulose	95.0 %	5.0 %	0	0	0

[#] represents the PALF sample has been pretreated for a thorough removal of fat, wax, water-soluble materials and pectin.

composition and physical properties of PALF, multiple linear regression analysis was employed to develop accurate predictive models. Specifically, predictive models along with residual plots were developed using multiple linear regression analysis implemented through MATLAB (Version R2023b, MathWorks, Inc.). Furthermore, this analysis was employed to investigate the relationships between various chemical components and the mechanical properties of PALF, including linear density, tenacity, Young's modulus, and tensile strain. In this way, the regression models were derived by fitting the data to a linear equation of the form:

$$Y = k_0 + k_1 X_1 + k_2 X_2 + ... + k_n X_n \#$$
 (2)

where Y represents the mechanical properties, and $X_1, X_2, ..., X_p$ correspond to the chemical compositions of the fiber, and $k, k_2, ..., k_p$ are the estimated regression coefficients, minimizing the residual sum of squares to obtain the best fit.

To further assess the goodness in fitting and the accuracy of the predictive models, residual plots were obtained from the above equations. These plots provided a visual check for any systematic deviations between the observed and predicted values, thereby allowing for the evaluation of model assumptions and the detection of potential outliers.

2.5. X-Ray diffraction (XRD)

To investigate the crystalline structure and crystallinity of PALF before and after degumming, X-ray diffraction (XRD) was employed and XRD patterns were recorded using a Bruker D8 Venture (German) at a scanning rate of 1°/min, covering a 2θ range from 5° to 90°. All fiber sample groups were then separately ground into powders to evaluate the impact of degumming on the fiber's structure.

The calculation of the crystal index (CI) was done by using peak height ratio (Segal method) as Eq. (3):

Crystal index
$$= \frac{I_{200} - I_{AM}}{I_{200}} \times 100\% \#$$
 (3)

where I_{200} corresponds to the integrated peak intensity of the (200) crystalline plane of cellulose I at 22.7° (2 θ), and I_{AM} represents the amorphous intensity derived from the cellulose I β phase at 18° (2 θ).

The crystallite size, τ perpendicular to the (200) lattice plane of cellulose I was determined by the Eq. (4) (Scherrer equation) to the full width at half maximum (FWHM) of the (200) diffraction peak at 22.7° (2 θ)

$$\tau = \frac{K\lambda}{\beta cos(\theta)} \# \tag{4}$$

where K is the correction factor (0.9), λ is the wavelength of the X-ray radiation (0.154056 nm), β is the FWHM of the diffraction peak in radians, and θ is the diffraction angle of the peak.

2.6. Surface morphology

Scanning electron microscope (Tescan VEGA3) was employed for the investigation of the morphological characteristics of single PALF. This analysis provides insights into the distribution of chemical components within the fiber, offering a deeper understanding of their influence on PALF's mechanical properties.

3. Results and discussion

3.1. Physical properties of single PALF

To simulate the effects of varying composition, morphology, and structure in PALF, the most widely cultivated Queen PALF was subjected to different degumming treatments. Individual fibers were isolated and tested until a minimum of 50 qualified specimens per group met acceptance criteria (valid fracture distance and cross-section). The physical properties of single Queen PALF are summarized in Table 2 and detailed data distributions were displayed in Fig. 1(a-d) for linear density, tensile strain, and Young's modulus.

3.1.1. Linear density

For the linear density, a decreasing trend was observed with the

Table 2 Physical properties of single Queen PALF under various degumming conditions.

Sample Group	Linear Density (dtex)	Tenacity (cN/ dtex)	Young's Modulus (GPa)	Tensile Strain (%)
SSD-1	21.57	5.14 ± 2.54	52.20	2.09
(Control group)	\pm 2.54		$\pm\ 13.67$	$\pm~0.65$
SSD-2	23.40	5.00 ± 1.24	41.05 ± 9.54	2.40
	\pm 5.86			$\pm~0.65$
SSD-3	23.00	3.77 ± 1.53	41.07	2.05
	\pm 7.56		$\pm~10.93$	$\pm~0.64$
SSD-4	20.59	2.18 ± 0.61	44.23	1.30
	\pm 5.47		± 11.64	± 0.41
SSD-5	20.33	1.23 ± 0.42	43.16 ± 6.39	0.74
	\pm 5.67			± 0.34
SSD-6	17.47	3.73 ± 1.10	34.60 ± 7.15	2.48
	\pm 6.19			$\pm~0.70$
SSD-7	18.05	3.77 ± 1.06	37.06 ± 9.26	2.48
	\pm 5.53			$\pm~0.64$
SSD-8	17.71	2.53 ± 1.55	34.52	2.00
	\pm 4.18		\pm 15.26	$\pm~0.64$
SSD-9	19.31	1.88 ± 0.68	43.92	1.21
	\pm 4.38		$\pm\ 14.41$	$\pm~0.43$
SSD-10	17.28	3.24 ± 1.11	37.05	2.56
	\pm 2.38		$\pm\ 14.27$	$\pm~0.85$
SSD-11	14.80	0.51 ± 0.17	25.03 ± 8.80	0.70
	$\pm~2.14$			± 0.56

^{*} represents the fat, wax and water-soluble materials in PALF.

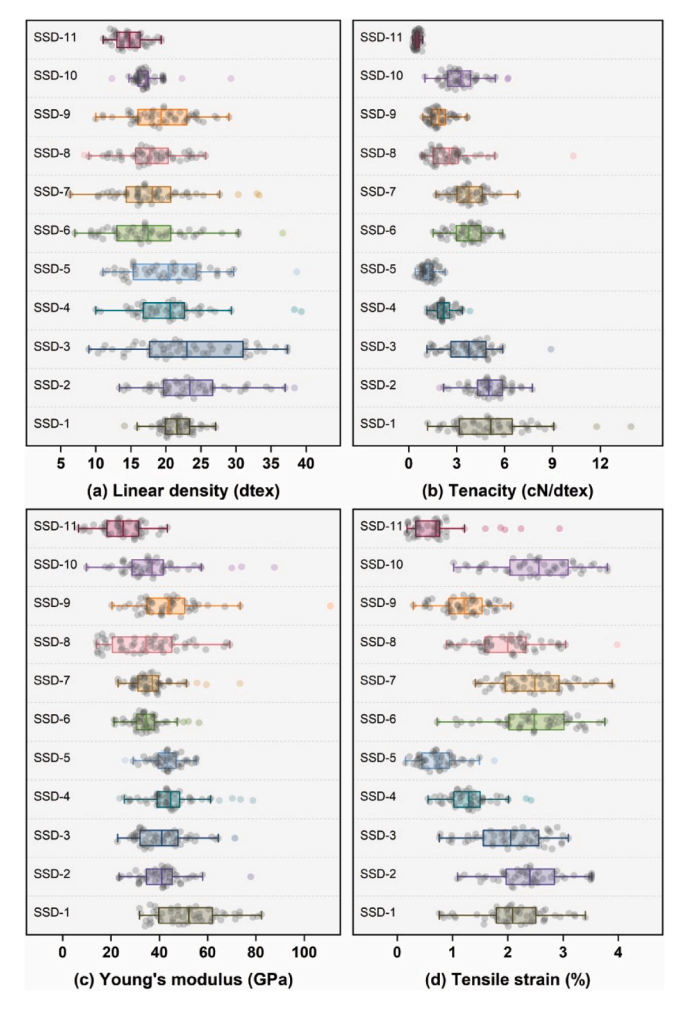


Fig. 1. Distribution of physical properties of single Queen PALF across degumming levels:(a) Linear density, (b) Tenacity, (c) Young's modulus and (d) Tensile strain. Box plots show the average, upper/lower quartiles, and outliers (\pm 1 SD).

reduction in hemicellulose content in Table 1, ranging from 21.57 \pm 2.54 dtex to 14.80 \pm 2.14 dtex. When hemicellulose within PALF was no more than 5 % (SSD-6/7/8/10), the average fineness decreased to around 17.5 dtex with an improvement of 18.9 %. This value is roughly equivalent to the combined thickness of 10 cotton fibers (~1.85 dtex, shown in Table 3) (Indra Doraiswamy and Chellamani, 1993). The SSD-11 group achieved a minimum fineness of 14.8 dtex yet exhibited severe mechanical degradation. Notably, its Young's modulus and tensile strain decreased by over 50 % compared to raw PALF, while tenacity plummeted to merely 10 % of the original value. This result is contrary to the well-known fact associating finer fibers with higher strength (Stoot, 1988). Such degradation was probably induced by the SSD-11's intensive degumming process, which removed all non-cellulosic components except 5 % hemicellulose, leading to the loss of inherent reinforced structure. As shown in Fig. 2, linear regression analysis demonstrated negligible correlations between fiber linear density and mechanical parameters. The coefficient of determination (R^2) for linear density versus tenacity was 0.58, and values for tensile strain and Young's modulus were below 0.5. These results conclusively exclude linear density as a viable predictor of PALF mechanical performance, which was distinct from the findings in ramie (Leng et al., 2023). Instead, as a natural fiber with complex gum constituents, PALF's mechanical behavior appears dominantly governed by the combined effects of chemical composition (e.g., residual gum content), morphological features, and structural characteristics.

Table 3
Comparison of physical properties of single Queen PALF with other natural fibers

Category	Linear Density (dtex)	Tenacity (cN/dtex)	Young's Modulus (GPa)	Tensile Strain (%)	Reference
Raw PALF (SSD-1)	21.57	5.14	52.20	2.09	Our work
Degummed PALF (SSD-10)	17.28	3.24	37.05	2.56	Our work
Cotton	1.85	3.30	7.48	7.50	(Abbott et al., 2010; VV et al., 2022)
Raw Jute	36.08	2.87	18	1.3	(George et al., 2001; Ray and Sarkar, 2001)
Raw Flax	17.50	4.67	27.6	3.0	(Aldroubi et al., 2023; George et al., 2001)
Raw Ramie	4.0–8.0	3.97–7.76	31.8	2.7	(Nam and Netravali, 2006; Roy, 2012)
Banana Fiber	56.0	2.93	27–32	1.0-3.0	(Balakrishnan et al., 2019)

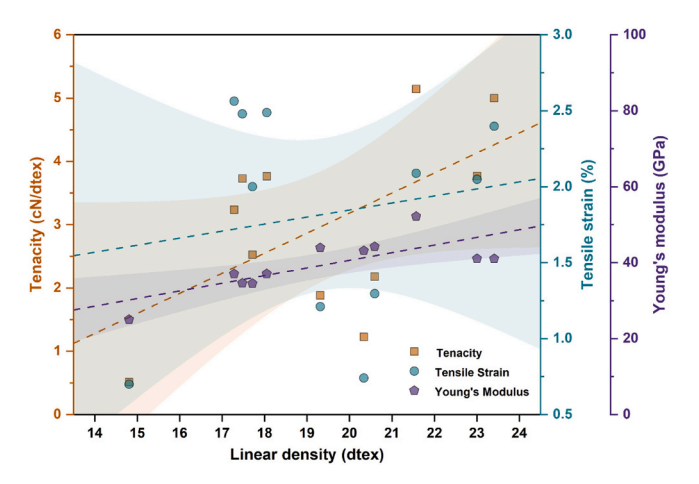


Fig. 2. Line regression analysis of single PALF's mechanical properties relationship with linear density. The orange line represents fiber's tenacity with linear density, fitted by the equation of y=-3.15+0.32x, $R^2=0.32$; The purple line represents fiber's Young's modulus with linear density, fitted by the equation of y=0.39+2.01x, $R^2=0.58$; The green line represents fiber's tensile strain with linear density, fitted by the equation of y=0.92+0.05x, $R^2=0.03$.

3.1.2. Tenacity

Lignin retention emerged as the dominant enhancer of fiber tensile strength among gums. SSD-2, which underwent the removal of fat and wax, maintained a strength close to the raw fiber (5.14 \pm 2.54 cN/dtex), outperforming cotton, jute and flax (George et al., 2001; VV et al., 2022). Progressive lignin removal (SSD-4/5/9) caused tenacity to decline proportionally, with complete delignification (SSD-5) reducing strength to 1.23 \pm 0.42 cN/dtex, approximately 43 % of the jute fiber (2.87 cN/dtex), shown in Table 3) (Ray and Sarkar, 2001). By comparing the SSD-9 (low lignin, high hemicellulose) and SSD-10 (high lignin, low hemicellulose), it confirmed lignin's superior impact: SSD-10 exhibited 72 % higher tenacity.

Hemicellulose regulation showed secondary influence. Groups with comparable residual hemicellulose (SSD-6/7) demonstrated consistent tenacity (\sim 3.7 cN/dtex), while its complete removal (SSD-8) caused a 32 % reduction (2.53 \pm 1.55 cN/dtex).

3.1.3. Young's modulus and tensile strain

Young's modulus followed distinct trends. All degummed PALFs still retained exceptional stiffness (~37.05 GPa), lower than raw PALF $(52.20 \pm 13.67 \text{ GPa})$ but higher than other natural fibers (< 35 GPa, Table 3). Previous studies have demonstrated that degumming enhances PALFs hydrophobicity and interfacial bonding (Lin, Tang, Huang, Yu, Li, et al., 2022; Shadhin et al., 2023; Todkar and Patil, 2019), contributing to improved composite strength. Tensile strain variability further highlighted lignin's role in flexibility. Raw PALF exhibited a tensile strain of 2.09 %, significantly lower than cotton (7.5 %), which partially explains its poor spinnability (Ismoilov et al., 2019). Fibers with reduced lignin content (SSD-4/5/9/11) showed lower elongation (1.2-1.8 %), whereas lignin-rich SSD-10 achieved 2.56 % strain, a 22.5 % increase compared to raw PALF. The selective removal of hemicellulose in SSD-10 creates microvoids between adjacent, highly oriented cellulose microfibrils, facilitating limited slippage when tensile force is applied along the fiber axis. At the same time, the rigid lignin framework acts as a reinforcing matrix, preventing the cellulose microfibrils from rupturing during deformation (Yang et al., 2019). This "slip-and-support" mechanism, where hemicellulose removal enables fibrillar mobility and lignin constrains structural collapse, results in enhanced elongation at break. Therefore, lignin plays an important role in stretching and absorbing stress before failure (Tang et al., 2024), improving PALF's toughness for applications requiring high elongation, such as impact-resistant biocomposites (Yang et al., 2019), elastic wearable textiles (Wu et al., 2023), and biodegradable packaging materials requiring controlled deformation under load (Jakob et al., 2022; Satyanarayana et al., 2009).

These findings emphasize the necessity of composition-based optimization for PALF rather than relying on empirical treatments. A more in-depth correlation analysis is warranted to fully elucidate the impact of each gum component on PALFs' physical properties, thereby providing valuable insights into material processing and industrial design.

3.2. Correlation analysis

The high cellulose content in PALF requires data normalization to mitigate analytical bias caused by its compositional dominance. Fig. 3 (a) shows the actual percentages of five components (cellulose, hemicellulose, lignin, pectin, and others) across degumming groups (SSD-1 to SSD-11) via 3D bars. To equalize component weights, data were normalized relative to SSD-1 (reference baseline), converting absolute

values into proportional ratios (Fig. 3(b)). This approach visually accentuates the compositional shifts of different samples while ensuring unbiased correlation analysis by assigning equal analytical weight to all components.

To better understand the interdependence among PALF's chemical components, Pearson's correlation matrix was used to examine the linear relationships between five primary components (cellulose, hemicellulose, lignin, pectin, and others), as shown in the triangular matrix of Fig. 4. The analysis revealed a strong negative correlation between hemicellulose and lignin (r=-0.65, p < 0.001), indicating that their concentrations in PALF tend to be mutually suppressed. Conversely, weak correlations (|r| < 0.5) were observed between other component pairs, such as pectin-hemicellulose, or hemicellulose-fat and wax, indicating minimal synergistic or dependent interactions. These findings highlight the feasibility for fine-tuning the individual component contents in degumming strategies.

The Mantel test was subsequently applied to evaluate the correlation between each chemical component and the physical properties, revealing that cellulose is the dominant driver of PALF's mechanical behavior, as summarized in Table 4. Cellulose content strongly correlated with linear density and Young's modulus (r = 0.78), confirming its pivotal role as the primary reinforcing phase within PALF (Komuraiah et al., 2014) and the key determinant of fiber's longitudinal stiffness (C. Zhang et al., 2021). Hemicellulose exhibited moderate positive correlations with linear density (r = 0.57) and Young's modulus (r = 0.43), attributable to its microfibril-coating network, which enhance interfiber adhesion through covalent linkages (e.g., ester/ether bonds) with lignin and pectin (Bourmaud et al., 2013; Youssefian and Rahbar, 2015; C. Zhang et al., 2021). As shown in Fig. 5(a), hemicellulose forms a membrane-like structure surrounding each fibril, thereby connecting individual fibrils into fiber bundles. Conversely, hemicellulose removal increased interfibrillar porosity, as evidenced by the cross-sectional morphology in Fig. 5(b), enabling fiber refinement at the cost of stiffness. This trade-off was also observed in bamboo fibrils. Molecular modeling studies on lignocellulosic systems reveal that hemicellulose networks, enriched with hydrogen-bonded polysaccharide chains, exhibit superior mechanical resilience compared to lignin-dominated matrices (Youssefian and Rahbar, 2015). Thus, hemicellulose residue serves as a critical level for balancing PALF's fineness and stiffness.

In terms of lignin, it emerged as the key mediator of PALF's stretchability among gums, showing the strongest correlation with tensile strain (r = 0.54). Its vertical cross-links between surface ravines (Fig. 5(c)) facilitate stress redistribution during stretching, whereas

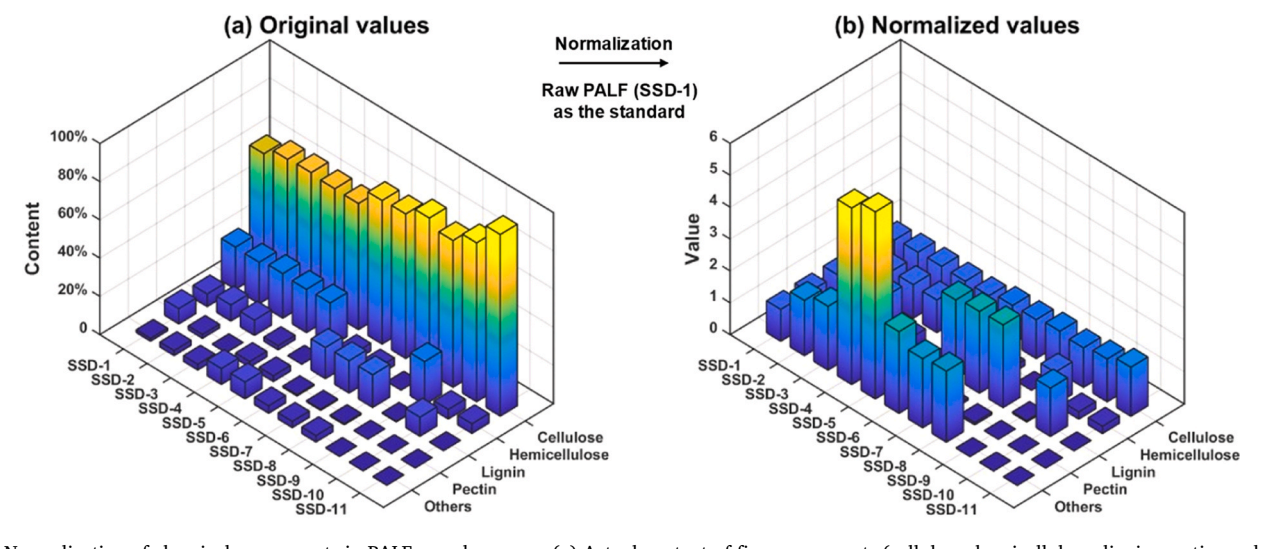


Fig. 3. Normalization of chemical components in PALF sample groups. (a) Actual content of five components (cellulose, hemicellulose, lignin, pectin, and others) across SSD-1 to SSD-11; (b) Normalized chemical composition values of sample groups. The color gradient, ranging from blue to yellow, indicates the content from low to high. "Others" represents fat, wax and water-soluble materials.

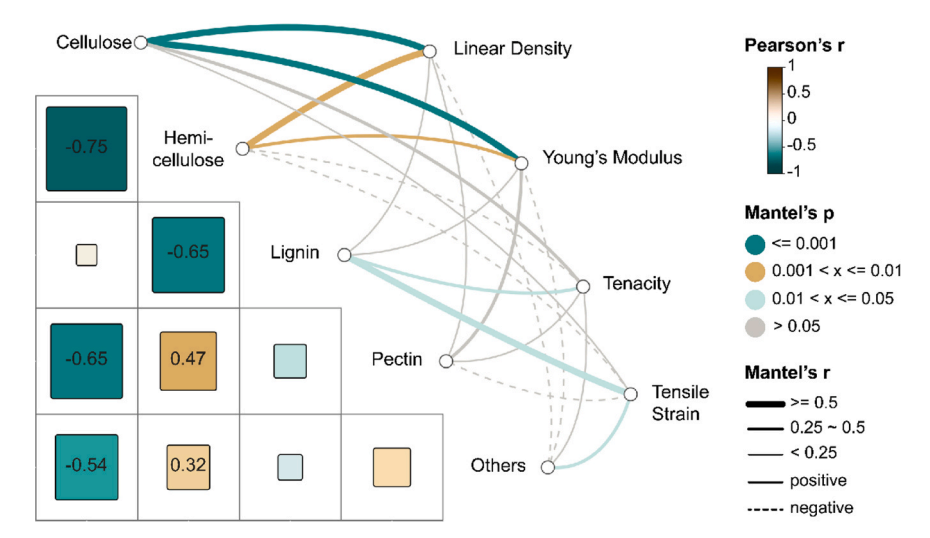


Fig. 4. Pearson's correlation matrix and Mantel tests illustrating the relationships between chemical components and physical properties of PALFs. Pearson's correlation coefficient matrix shows the relationships among chemical components, with green and brown indicating negative and positive correlations, respectively. The significant level of Pearson's correlations is represented by the square size, with a higher coefficient (closer to +1 or -1) indicating a stronger positive or negative relationship, while values near 0 imply weak or no correlation. The Mantel test quantifies the correlation between chemical components with physical properties (linear density, Young's modulus, tenacity, and tensile strain). The positive and negative correlations are respectively displayed in solid and dash lines. Line width corresponds to the Mantel's r value and line color reflects the statistical p value; green, brown, light green and gray represent significant levels of ≤ 0.001 , ≤ 0.01 , ≤ 0.05 , and > 0.05, respectively. Gray lines (p > 0.05) indicate that the correlation cannot be clearly determined in the current data, while lines in other colors signify statistical significance. "Others" represents fat, wax and water-soluble materials in PALFs.

Table 4 Mantel test correlation coefficients (Mantel's r) between chemical components and physical properties of PALFs.

Components	Linear Density	Tenacity	Young's Modulus	Tensile Strain	Sum of Mantel's r
Cellulose	0.78	0.48	0.78	0.19	2.23
Hemicellulose	0.57	-0.08	0.43	-0.04	1.12
Lignin	0.06	0.28	0.16	0.54	1.04
Pectin	0.05	0.02	0.34	-0.13	0.54
Others	-0.08	0.19	-0.03	0.32	0.62

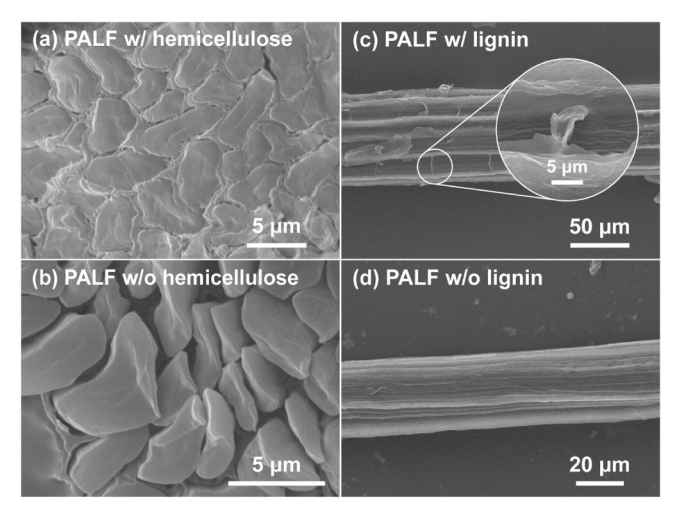


Fig. 5. Morphological characterization of PALF with different chemical components. (a) Cross-section of PALF retaining hemicellulose (SSD-2); (b) Cross-section of PALF without hemicellulose (SSD-8); (c) Surface of PALF retaining lignin (SSD-2); (d) Surface of PALF without lignin (SSD-9).

delignification eliminates these bridges (Fig. 5(d)), reducing elongation by 50 %. Additionally, other gum residues (fat, wax and water-soluble materials) exhibit weak positive correlation with tensile strain ($r = \frac{1}{2}$)

0.32) and tenacity (r=0.19), likely due to their small amounts in the S2 layer of the secondary wall structure within single PALF (Sadrmanesh and Chen, 2019). This layer is critical for determining fiber mechanical properties.

Overall, the Mantel test results establish a hierarchical componentfunction framework: cellulose, with its crystalline microfibrils, governs fiber stiffness and fineness as the main reinforcing component; lignin enhances stretchability and strength via stress-transfer structure; and hemicellulose modulates fiber fineness and interfacial adhesion as primary part of the bonding network. Degumming optimization of this triad enables the tailoring of PALF for applications ranging from high-stiffness composites to flexible textiles.

3.3. Prediction models construction and analysis

3.3.1. Overview of the PFS-PALF model composition

The PFS-PALF predictive framework comprises four target physical properties (linear density, Young's modulus, tenacity, and tensile strain), each modeled as a function of five compositional parameters (X_1 : cellulose, X_2 : hemicellulose, X_3 : lignin, X_4 : pectin, X_5 : fat, wax and water soluble materials). Multivariate regression coefficients were derived from the correlation matrix to yield separate equations for each property, all exhibiting $R^2 \geq 0.9$ (p < 0.05) as follows, confirming the statistical significance and excellent fit of the models.

$$Y_L = 7.923X_1 + 10.243X_2 + 2.573X_3 + 0.911X_4 + 0.12X_5\#$$
 (5)

$$Y_T = -0.193X_1 + 2.653X_2 + 1.578X_3 + 1.564X_4 - 0.298X_5\#$$
 (6)

$$Y_{M} \ = \ 16.268 X_{1} \ + \ 19.046 X_{2} \ + \ 4.54 X_{3} \ + \ 11.97 X_{4} \ + \ 0.094 X_{5} \# \eqno(7)$$

$$Y_S \ = \ 0.385 X_1 \ + \ 0.92 X_2 \ + \ 0.822 X_3 \ + \ 0.141 X_4 \ \text{-} \ 0.106 X_5 \# \eqno(8)$$

As shown in the residual fitting plots (Fig. 6), residual analysis assessed the models' robustness, with >90 % residuals were centered around zero, confirming that the assumptions of linearity and homoscedasticity are met. Although these fitting results indicate that structure changes are implicitly captured by the current models, the explicit

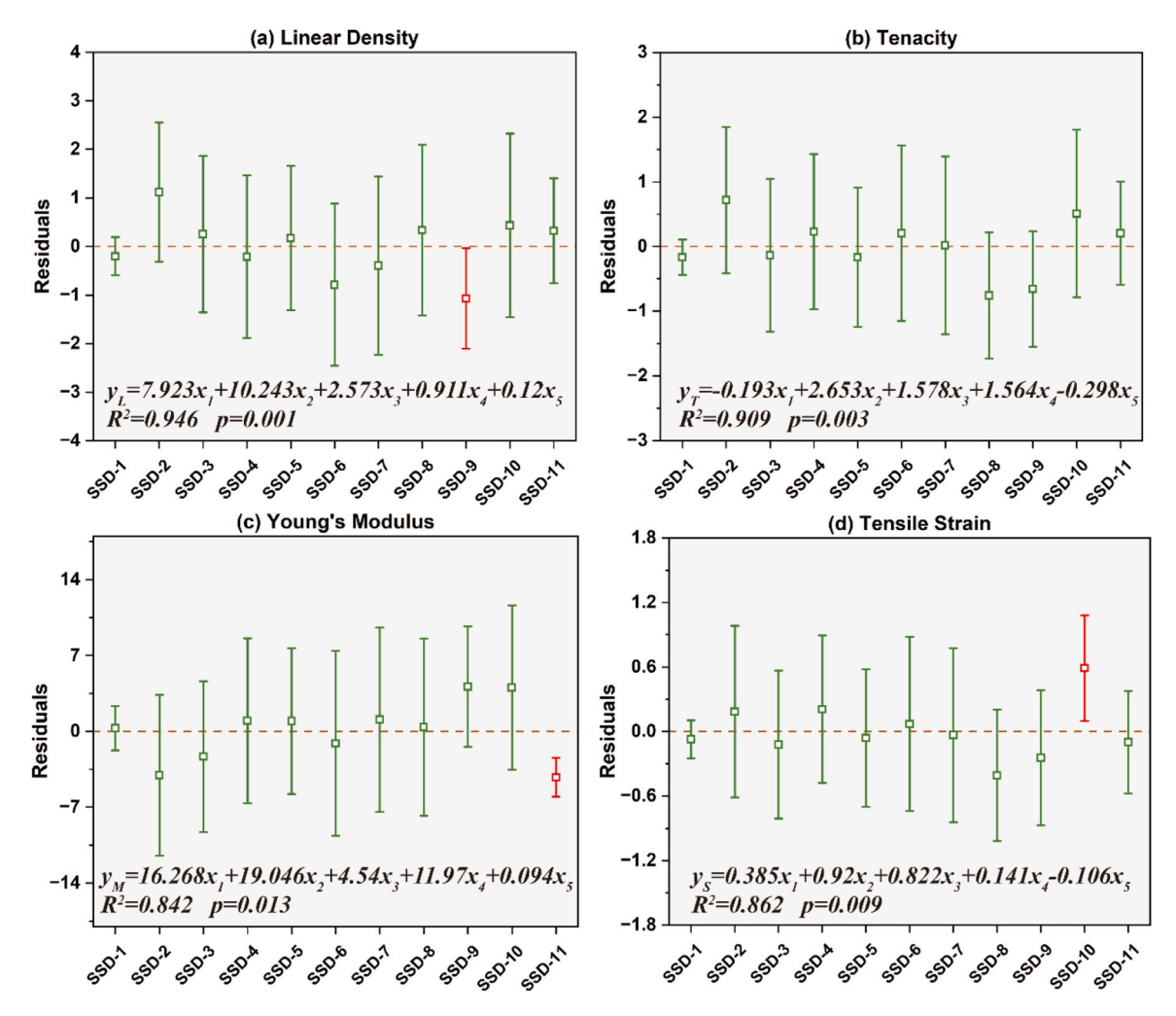


Fig. 6. The PFS-PALF predictive equations with corresponding residual plots for fineness and tensile properties of single PALF.

incorporation of crystal parameters could further enhance predictive accuracy—a promising direction for future model optimization.

3.3.2. PALF structure analysis

The regression coefficients of predictors in the computational models do not strictly align with their Mantel correlation rankings. For instance, cellulose (X_1) does not receive the highest weight in the model despite its primary compositional influence. This discrepancy arises from structural rearrangement during chemical degumming; cellulose microfibrils may stretch, curve, reorient, degrade or bundle with other adjacent microfibrils, significantly impacting the fiber's mechanical behavior (Lin, Tang, Huang, Yu, Yu, et al., 2022; Zhang et al., 2021). Thus, structural parameters such as crystal index (CI) and crystallize size also changed.

As shown in Fig. 7 and Table 5, XRD results of PALF powders subjected to different degumming treatments, along with calculated CI and crystal size, demonstrate good structure-property relationship. For the raw PALF (SSD-1, 61.9% cellulose), moderate peak intensities at 22.5° (200), $15^{\circ}(1-10)$, $16^{\circ}(100)$ indicate highly ordered crystalline regions within the cellulose microfibrils, with a CI of 62.78% and a (200) crystal size of 2.86 nm. By contrast, SSD-10 (83.1% cellulose, 10% lignin, 5.0% hemicellulose) exhibits the sharpest (200) peak, yielding higher CI (72.58%) but reduced crystal size (2.39 nm); this size-induced embrittlement correlates with tenacity loss (3.24 cN/dtex) and Young's modulus decline (37.05 GPa). SSD-11 represents an extreme case where nearly pure cellulose is achieved (95% cellulose, 5.0% hemicellulose), yet the CI unexpectedly drops to 67.26%. This likely

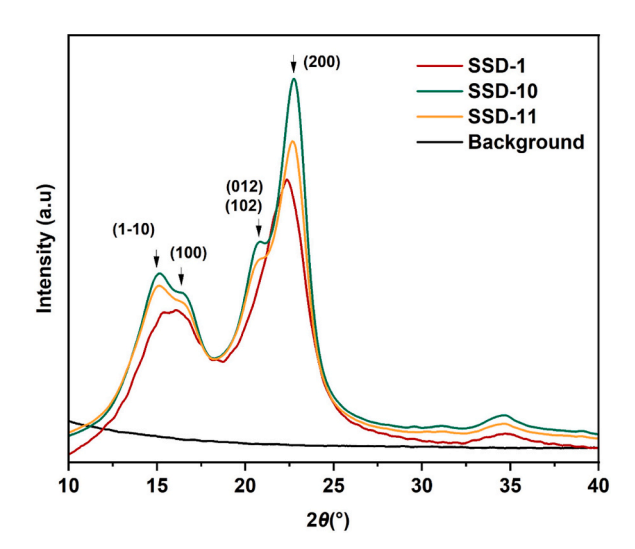


Fig. 7. X-ray diffraction results of dry PALF powders subjected to varying degumming levels, with the baseline representing air scattering background without cellulose.

stems from cellulose polymorphism transitions or crystalline domain degradation during excessive degumming (Jose et al., 2016). Concurrently, disrupted hydrogen bonding networks severely weaken interfibrils' cohesion (Ma et al., 2012), causing mechanical collapse (tenacity:

Table 5Crystalline information of PALF subjected to varying degumming levels.

Sample group	Crystal index	Crystal size (Cellulose I β) nm		
	(Cellulose I β)	200	1–10	100
SSD-1	62.78 %	2.86	0.69	3.15
SSD-10	72.58 %	2.39	1.91	0.33
SSD-11	67.26 %	2.72	1.81	0.68

0.51 cN/dtex; modulus: 25.03 GPa). Despite retaining a (200) crystal size of 2.72 nm, over-degumming also altered the internal crystal orientation, amplifying amorphous regions that act as preferential failure sites (Ahmed et al., 2022; Lin, Tang, Huang, Yu, Yu, et al., 2022). These structural defects synergistically compromise stress distribution and interfacial cohesion, ultimately degrading fiber integrity.

3.4. Model validation and PALF performance assessment

3.4.1. Model validation

A novel degummed PALF group (SSD-12) with high lignin (13.0 %) and minimized hemicellulose (3.0 %) was developed based on correlation analysis. The preparation followed a modified stepwise degumming method, wherein alkali concentration was reduced from 20 to 5 g/L coupled with expanded treatment duration from 2 to 5 h in step3 to preserve cellulose integrity (Liao et al., 2025). Compared to the prior optimal group (SSD-1), SSD-12 exhibited superior mechanical performance: tenacity increased by 26 % (4.06 vs. 3.24 cN/dtex), Young's modulus rose by 13 % (42.01 vs. 37.05 GPa), tensile strain improved by 4.7 % (2.68 vs. 2.56 cN/dtex), while maintaining refined fineness (below 17.5 dtex), validating targeted composition-driven fiber enhancement.

To validate the PFS-PALF model's generalizability, the properties of three additional PALF varieties (MD-2, Red Spanish, Smooth Cayenne) were analyzed, with their chemical compositions detailed in Table 6. Comparisons between measured and predicted values for all sample groups (including SSD1–12) are shown in Fig. 8(a-d). Predictions for fineness and tensile properties demonstrated high accuracy, with most experimental data aligning well with predicted results. Minor deviations fell within the SD range of the measuring results. Paired T-tests confirmed no statistically significant differences between the datasets at a 95 % confidence interval. The detailed p-values for the four properties: $p_L=0.682, p_T=0.581, p_M=0.886, \ p_S=0.734$, exceeded 0.05. Linear regressions of measured (x-axis) versus predicted (y-axis) values yielded fitted lines near y=x (R² ≥ 0.9), as shown in Fig. 8(e-h), further validating the PFS-PALF model as a reliable predictor of single PALF's fineness and strength.

 $\begin{tabular}{ll} \textbf{Table 6} \\ \textbf{Chemical components of validated fiber groups and normalization (SSD-12, MD-2, Red Spanish, and Smooth Cayenne PALF).} \end{tabular}$

Measured Chemical Components (%)							
	Cellulose	Hemicellulose	Lignin	Pectin	Others		
SSD-1 (Standard Baseline)	61.9 %	22.1 %	6.6 %	8.0 %	1.5 %		
SSD-12 (Optimized Degumming group)	80.1 %	3.0 %	13.0 %	3.9 %	0		
MD-2	30.4 %	34.5 %	4.6 %	16.7 %	13.8 %		
Red Spanish	48.3 %	38.0 %	4.5 %	2.0 %	7.30 %		
Smooth Cayenne	62.7 %	28.2 %	5.8 %	0.9 %	2.40 %		
Normalized Value of Chemical Components							
SSD-12	1.294	0.136	1.97	0.488	0.000		
MD-2	0.491	1.561	0.697	2.088	9.200		
Red Spanish	0.780	1.719	0.682	0.250	4.867		
Smooth Cayenne	1.013	1.2276	0.879	0.113	1.600		

3.4.2. Performance ranking of PALF varieties

In addition, the PFS-PALF model enabled rapid performance ranking across PALF varieties, which will be beneficial for application-oriented material selection. MD-2 with the highest tensile strength and Young's modulus (5.5 cN/dtex, 72 GPa) is optimal for load-bearing composites, such as automotive panels and construction reinforcement (Jawaid et al., 2020). Queen has superior tensile strain (2.09 %) and minimum linear density (21.57 dtex), ideal for flexible textiles (medical gauze, sportswear) and impact-absorbing biocomposites (Mishra et al., 2004). Smooth Cayenne and Red Spanish PALF with moderate properties, may be suitable for cost-sensitive bulk materials after targeted processing.

Performance ranking of PALF varieties as below:

- Linear density: MD-2 > Red Spanish > Smooth Cayenne > Queen
- Tenacity: MD-2 > Queen > Red Spanish > Smooth Cavenne
- Young's modulus: MD-2 > Queen > Red Spanish > Smooth Cayenne
- Tensile strain: Queen > Smooth Cayenne > Red Spanish > MD-2

4. Conclusion and outlook

This study establishes a quantitative framework (PFS-PALF) that links the chemical compositions of single PALF to their mechanical performance across varying degrees of degumming, enabling precise prediction of PALF fineness, tenacity, and modulus. Pearson and Mantel correlation analyses revealed a hierarchical structure-function relationship: cellulose governs stiffness and fineness through its crystalline packing, hemicellulose regulates fineness and interfacial adhesion via bonding networks, and lignin enhances flexibility and strength through stress-transfer structure. Degumming not only alters the cellulose-tonon-cellulosic ratio but also affects fiber structure, thereby influencing mechanical integrity by disrupting microfibril cohesion. The PFS-PALF model effectively integrates these compositional and structural changes into its calculation coefficients, achieving high predictive accuracy across 15 sample groups with no statistically significant differences compared to standard testing methods at a 95 % confidence interval. It enables fast, high-throughput evaluation of raw materials without the need for specialized tensile equipment or tedious sample preparation, making it particularly suitable for real-time quality control in industrial applications.

Furthermore, the model facilitates an inverse regulation of the degumming parameters to produce PALF with optimized chemical compositions for superior tensile strength and fineness. It also enables rapid performance ranking across different PALF varieties, supporting the selection of suitable fibers for application-specific mechanical thresholds. For instance, MD-2 PALF is optimal for composites that demand high stiffness and strength, whereas Queen PALF is well-suited for textiles and impact-absorbing biocomposites that require enhanced flexibility.

Building on these findings, future research should integrate multiscale structural parameters—such as crystallinity index, crystallite size, and microfibril orientation—into predictive algorithms to further refine structure—property correlations. Additionally, given that over 70 pineapple varieties exist globally, establishing an open-access fiber database paired with AI-driven processing recommendations will be invaluable for advancing the industrial application of PALF. These advancements will accelerate the transition from empirical processing to intelligent material design, positioning PALF as a cornerstone of sustainable manufacturing across biomedical, composite, and textile industries.

CRediT authorship contribution statement

Xungai Wang: Writing – review & editing, Supervision, Resources, Project administration, Funding acquisition, Conceptualization. Jianming Chen: Writing – review & editing, Methodology, Formal analysis, Data curation. Shiyu Liao: Writing – original draft, Methodology, Investigation, Formal analysis, Data curation.

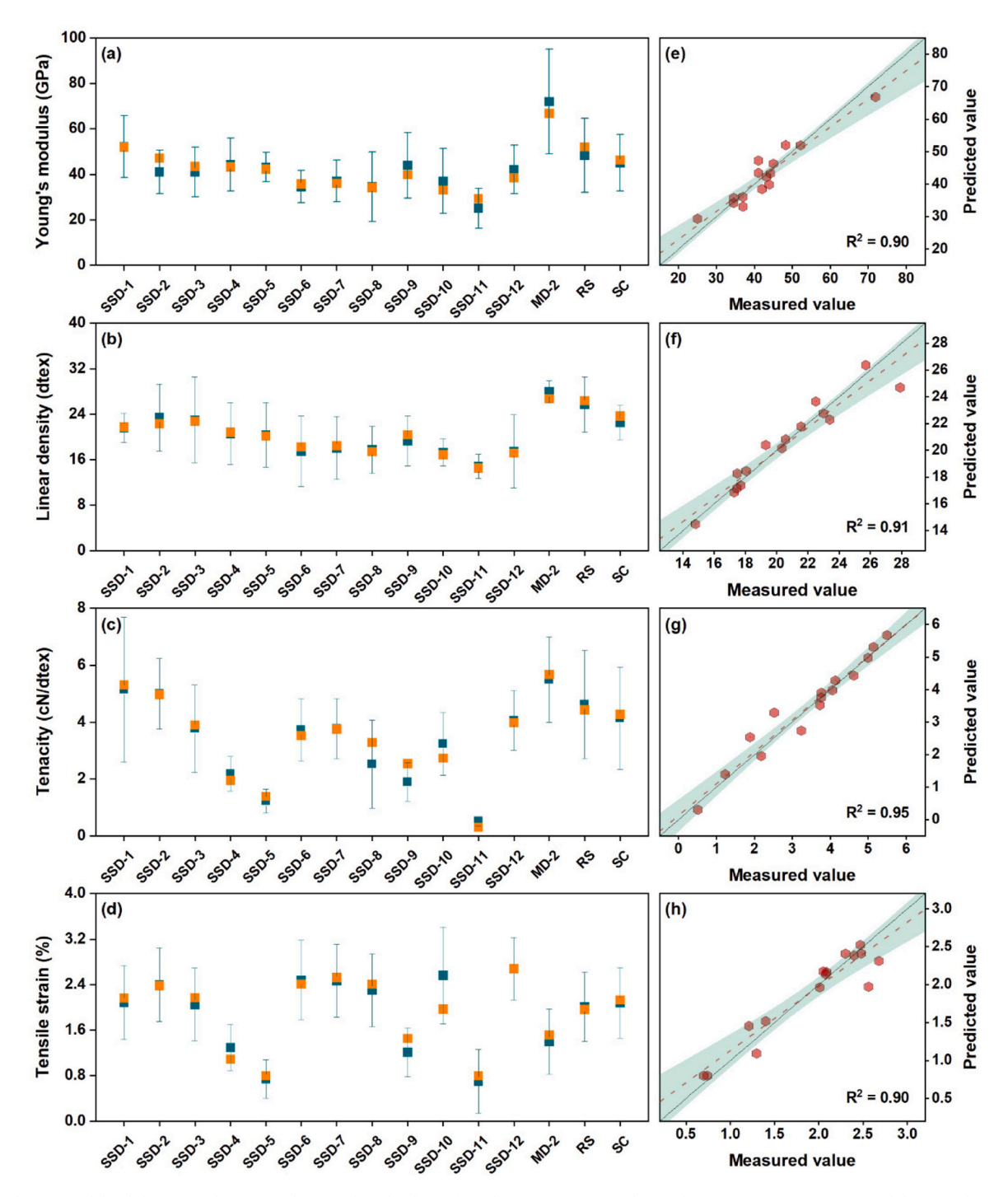


Fig. 8. Predictive model validation: (a-d) Measured vs. predicted values of single PALF properties (linear density, tenacity, Young's modulus, tensile strain) across degumming groups (SSD-1 to SSD-12) and cultivars (SSD-1/Queen, MD-2, Red Spanish, Smooth Cayenne); (e-h) Corresponding fitted regression lines (dashed lines) against the ideal y = x relationship (solid lines), demonstrating model fidelity.

Declaration of Competing Interest

The authors declare that they have no known competing financial interests or personal relationships that could have appeared to influence the work reported in this paper.

Acknowledgement

This work was supported by the Joint Research Centre for Fiber Innovations and Renewable Materials and Research Centre of Textiles for Future Fashion at the Hong Kong Polytechnic University.

Data availability

Data will be made available on request.

References

Abbott, A., Higgerson, G., Long, R., Lucas, S., Naylor, G., Tischler, C., Purmalis, M., 2010. An instrument for determining the average fiber linear density (fineness) of cotton lint samples. Text. Res. J. 80 (9), 822–833. https://doi.org/10.1177/0040517509348335.

- Ahmed, B., Wu, Q., Lin, H., Gwon, J., Negulescu, I., Cameron, B., 2022. Degumming of hemp fibers using combined microwave energy and deep eutectic solvent treatment. Ind. Crops Prod. 184, 115046. https://doi.org/10.1016/j.indcrop.2022.115046.
- Aldroubi, S., Kasal, B., Yan, L., Bachtiar, E.V., 2023. Multi-scale investigation of morphological, physical and tensile properties of flax single fiber, yarn and unidirectional fabric. Compos. Part B Eng. 259, 110732. https://doi.org/10.1016/j. compositesb.2023.110732.
- Balakrishnan, S., Wickramasinghe, G., Wijayapala, U.S., 2019. Investigation on improving banana fiber fineness for textile application. Text. Res. J. 89 (21-22), 4398–4409. https://doi.org/10.1177/0040517519835758.
- Bourmaud, A., Morvan, C., Bouali, A., Placet, V., Perre, P., Baley, C., 2013. Relationships between micro-fibrillar angle, mechanical properties and biochemical composition of flax fibers. Ind. Crops Prod. 44, 343–351. https://doi.org/10.1016/j. indcrop.2012.11.031.
- Chollakup, R., Tantatherdtam, R., Ujjin, S., Sriroth, K., 2011. Pineapple leaf fiber reinforced thermoplastic composites: Effects of fiber length and fiber content on their characteristics. J. Appl. Polym. Sci. 119 (4), 1952–1960. https://doi.org/ 10.1002/app.32910.
- Gaba, E.W., Asimeng, B.O., Kaufmann, E.E., Katu, S.K., Foster, E.J., Tiburu, E.K., 2021. Mechanical and structural characterization of pineapple leaf fiber. Fibers 9 (8), 51. https://doi.org/10.3390/fib9080051.
- George, J., Sreekala, M., Thomas, S., 2001. A review on interface modification and characterization of natural fiber reinforced plastic composites. Polym. Eng. Sci. 41 (9), 1471–1485. https://doi.org/10.1002/pen.10846.
- Han, J., Du, M., Huang, Y., Fu, S., Yu, J., Li, Z., Ding, B., 2024. Hierarchical nanoengineered emulsion with robust adhesion enables superior self-cleaning cotton fabrics. Text. Res. J. 94 (17-18), 1988–2000. https://doi.org/10.1177/ 0040517524124109.
- $\label{localized-local} Indra \ Doraiswamy, I.D., \ Chellamani, P., \ 1993. \ Pineapple-Leaf \ Fibres. \ https://doi.org/https://doi.org/10.5555/19940307777.$
- Ismoilov, K., Chauhan, S., Yang, M., Heng, Q., 2019. Spinning system for pineapple leaf fiber via cotton spinning system by solo and binary blending and identifying yarn properties. J. Text. Sci. Technol. 5 (4), 86–91. https://doi.org/10.4236/ itst 2019 54008
- Jakob, M., Mahendran, A.R., Gindl-Altmutter, W., Bliem, P., Konnerth, J., Müller, U., Veigel, S., 2022. The strength and stiffness of oriented wood and cellulose-fibre materials: a review. Prog. Mater. Sci. 125, 100916. https://doi.org/10.1016/j. pmatsci.2021.100916.
- Jawaid, M., Asim, M., Tahir, P.M., Nasir, M., 2020. Pineapple leaf fibers. Green. Energy Technol. https://doi.org/10.1007/978-981-15-1416-6.
- Jose, S., Salim, R., Ammayappan, L., 2016. An overview on production, properties, and value addition of pineapple leaf fibers (PALF). J. Nat. Fibers 13 (3), 362–373. https://doi.org/10.1080/15440478.2015.1029194.
- Komuraiah, A., Kumar, N.S., Prasad, B.D., 2014. Chemical composition of natural fibers and its influence on their mechanical properties. Mech. Compos. Mater. 50, 359–376. https://doi.org/10.1007/s11029-014-9422-2.
- Leng, J., Xiao, A., Liu, L., Liao, L., Feng, X., 2023. Construction and application of regression model for breaking strength of ramie single fiber. Farm Prod. Process. 7, 1671–9646. https://doi.org/10.16693/j.cnki.1671-9646(X).2023.07.013.
- Liao, S., Chen, J., Li, L., Li, P., Wang, X., 2025. Stepwise degumming of pineapple leaf fibers with tunable fineness and excellent antibacterial property. Ind. Crops Prod. 225, 120490.
- Lin, G., Tang, Q., Huang, H., Yu, C., Yu, J., Li, Z., Ding, B., 2022. One-step extraction of ramie cellulose fibers and reutilization of degumming solution. Text. Res. J. 92 (19-20), 3579–3590. https://doi.org/10.1177/00405175221086886.
- Lin, G., Tang, Q., Huang, H., Yu, J., Li, Z., Ding, B., 2022. Process optimization and comprehensive utilization of recyclable deep eutectic solvent for the production of ramie cellulose fibers. Cellulose 29 (7), 3689–3701. https://doi.org/10.1007/ s10570-022-04501-0.
- Ma, Y.H., Lin, F.D., Wang, B.G., Tong, J., Jia, H.L., 2012. The mechanical properties of natural fiber. Adv. Mater. Res. 487, 29–32. https://doi.org/10.4028/www.scientific. net/AMR.487.29.
- Manaia, J.P., Manaia, A.T., Rodriges, L., 2019. Industrial hemp fibers: an overview. Fibers 7 (12), 106. https://doi.org/10.3390/fib7120106.
- Mazumder, S., Zhang, N., 2023. Cellulose–hemicellulose–lignin interaction in the secondary cell wall of coconut endocarp. Biomimetics 8 (2), 188. https://doi.org/ 10.3390/biomimetics8020188.
- Mishra, S., Mohanty, A.K., Drzal, L.T., Misra, M., Hinrichsen, G., 2004. A review on pineapple leaf fibers, sisal fibers and their biocomposites. Macromol. Mater. Eng. 289 (11), 955–974. https://doi.org/10.1002/mame.200400132.
- Nam, S., Netravali, A.N., 2006. Green composites. I. Physical properties of ramie fibers for environment-friendly green composites. Fibers Polym. 7, 372–379. https://doi. org/10.1007/BF02875769.
- Neto, A.R.S., Araujo, M.A., Barboza, R.M., Fonseca, A.S., Tonoli, G.H., Souza, F.V., Mattoso, L.H., Marconcini, J.M., 2015. Comparative study of 12 pineapple leaf fiber

- varieties for use as mechanical reinforcement in polymer composites. Ind. Crops Prod. 64, 68-78. https://doi.org/10.1016/j.indcrop.2014.10.042.
- Neto, A.R.S., Araujo, M.A., Souza, F.V., Mattoso, L.H., Marconcini, J.M., 2013. Characterization and comparative evaluation of thermal, structural, chemical, mechanical and morphological properties of six pineapple leaf fiber varieties for use in composites. Ind. Crops Prod. 43, 529–537. https://doi.org/10.1016/j.indcrop.2012.08.001.
- Radoor, S., Karayil, J., Rangappa, S., Siengchin, S., Parameswaranpillai, J., 2020.
 A review on the extraction of pineapple, sisal and abaca fibers and their use as reinforcement in polymer matrix. Express Polym. Lett. 14 (4), 309–335. https://doi.org/10.3144/expresspolymlett.2020.27.
- Ray, D., Sarkar, B., 2001. Characterization of alkali-treated jute fibers for physical and mechanical properties. J. Appl. Polym. Sci. 80 (7), 1013–1020.
- Roy, S., L. B. L, 2012. Bast Fibres: Ramie. Woodhead Publishing. https://doi.org/ 10.1016/B978-0-12-818398-4.00004-9.
- Sadrmanesh, V., Chen, Y., 2019. Bast fibres: structure, processing, properties, and applications. Int. Mater. Rev. 64 (7), 381–406. https://doi.org/10.1080/ 09506608.2018.1501171.
- Satyanarayana, K.G., Arizaga, G.G., Wypych, F., 2009. Biodegradable composites based on lignocellulosic fibers—an overview. Prog. Polym. Sci. 34 (9), 982–1021. https:// doi.org/10.1016/j.progpolymsci.2008.12.002.
- Shadhin, M., Rahman, M., Jayaraman, R., Chen, Y., Mann, D., Zhong, W., 2023. Natural biomass & waste biomass fibers–structures, environmental footprints, sustainability, degumming methods, & surface modifications. Ind. Crops Prod. 204, 117252. https://doi.org/10.1016/j.indcrop.2023.117252.
- Shen, P., Tang, Q., Chen, X., Li, Z., 2022. Nanocrystalline cellulose extracted from bast fibers: Preparation, characterization, and application. Carbohydr. Polym. 290, 119462. https://doi.org/10.1016/j.carbpol.2022.119462.
- Sinon, F.G., Kohler, R., Cotter, M., Mueller, J., 2011. Tenacity, fineness and ultimate fiber recovery of abaca fiber strands. J. Biobased Mater. Bioenergy 5 (4), 433–441. https://doi.org/10.1166/jbmb.2011.1129.
- Smitthipong, W., Tantatherdtam, R., Chollakup, R., 2015. Effect of pineapple leaf fiber-reinforced thermoplastic starch/poly (lactic acid) green composite: mechanical, viscosity, and water resistance properties. J. Thermoplast. Compos. Mater. 28 (5), 717–729. https://doi.org/10.1177/0892705713489701.
- Stoot, P.H. 1988. Fiber and Yarn Quality In Jute Spinning: An Account Of Fibers-on-machinery: Research Work. Textile Institute. (https://libraryopac.nust.ac.zw/cgi-bin/koha/opac-detail.pl?biblionumber=162655&shelfbrowse_itemnumber=158378).
- Surajarusarn, B., Traiperm, P., Amornsakchai, T., 2019. Revisiting the morphology, microstructure, and properties of cellulose fibre from pineapple leaf so as to expand its utilization. Sains Malays. 48, 145–154. https://doi.org/10.17576/jsm-2019-4801-17.
- Tang, Q., Chen, Y., Du, M., Yu, J., Li, Z., Ding, B., 2024. Research progress in Ramie fiber extraction: Degumming method, working mechanism, and fiber performance. Ind. Crops Prod. 222, 119876. https://doi.org/10.1016/j.indcrop.2024.119876.
- Teles, M.C.A., Glória, G.O., Altoé, G.R., Amoy Netto, P., Margem, F.M., Braga, F.O., Monteiro, S.N., 2015. Evaluation of the diameter influence on the tensile strength of pineapple leaf fibers (PALF) by Weibull method. Mater. Res. 18, 185–192. https://doi.org/10.1590/1516-1439.362514
- Todkar, S.S., Patil, S.A., 2019. Review on mechanical properties evaluation of pineapple leaf fibre (PALF) reinforced polymer composites. Compos. Part B Eng. 174, 106927. https://doi.org/10.1016/j.compositesb.2019.106927.
- VV, M., S, D., Narayan Hegde, V., 2022. Structural and elastic properties of varieties of cotton fibers. Adv. Mater. Process. Technol. 8 (4), 3990–4006. https://doi.org/ 10.1080/2374068X 2022 2036502
- Wang, W.-m, Cai, Z.-s, Yu, J.-y, Xia, Z.-p, 2009. Changes in composition, structure, and properties of jute fibers after chemical treatments. Fibers Polym. 10, 776–780. https://doi.org/10.1007/s12221-009-0776-3.
- Wu, Y., Tang, J., Ma, S., Zhang, K., Yan, T., Pan, Z., 2023. A review of flexible strain sensors based on natural fiber materials. Adv. Mater. Technol. 8 (7), 2201503. https://doi.org/10.1002/admt.202201503.
- Yang, J., Ching, Y.C., Chuah, C.H., 2019. Applications of lignocellulosic fibers and lignin in bioplastics: a review. Polymers 11 (5), 751. https://doi.org/10.3390/ polym11050751.
- Youssefian, S., Rahbar, N., 2015. Molecular origin of strength and stiffness in bamboo fibrils. Sci. Rep. 5 (1), 11116.
- Zhang, C., Chen, M., Keten, S., Coasne, B., Derome, D., Carmeliet, J., 2021. Hygromechanical mechanisms of wood cell wall revealed by molecular modeling and mixture rule analysis. Sci. Adv. 7 (37), eabi8919. https://doi.org/10.1126/ sciadv.abi8919.
- Zhang, Y., Yu, J., Wang, X., Durachko, D.M., Zhang, S., Cosgrove, D.J., 2021. Molecular insights into the complex mechanics of plant epidermal cell walls. Science 372 (6543), 706–711. https://doi.org/10.1126/science.abf2824.